Photoluminescence, thermoluminescence and EPR studies on $Zn_4B_6O_{13}$

1990 J. Phys.: Condens. Matter 2 6303

(http://iopscience.iop.org/0953-8984/2/29/008)

J. Phys.: Condens. Matter 2 (1990) 6303–6313. Printed in the UK

Photoluminescence, thermoluminescence and EPR studies on $Zn_4B_6O_{13}$

A Meijerink†, G Blasse† and M Glasbeek‡

† Debye Research Institute, University of Utrecht, PO Box 80 000, 3508 TA Utrecht, The Netherlands

‡ Laboratory for Physical Chemistry, University of Amsterdam, Nieuwe Achtergracht 127, 1018 WS Amsterdam, The Netherlands

Received 31 January 1990, in final form 17 April 1990

Abstract. Photoluminescence, thermoluminescence and temperature dependent EPR measurements on $Zn_4B_6O_{13}$ are reported and discussed. The photoluminescence properties show that the intrinsic violet emission of this compound may originate from a strongly localised self-trapped exciton state. Four types of UV-induced paramagnetic centres are identified on the basis of g-values and hyperfine splitting, namely electrons trapped in two types of oxygen vacancies, electrons trapped on or near Mn^{2+} impurities and holes trapped by borate groups. The thermal decay of the paramagnetic centres is discussed in relation to the thermoluminescence.

1. Introduction

For the study of radiation-induced paramagnetic centres EPR has proven to be a very suitable technique [1]. The created paramagnetic defects can be identified on the basis of g-values and hyperfine splitting parameters. A combined study of the photoluminescence, thermoluminescence and temperature dependent EPR spectra yields information on the thermal stability and nature of radiation-induced paramagnetic centres.

Much research has been performed on radiation-induced paramagnetic centres in the borate framework of alkali borate glasses [2–4]. Most EPR studies on crystalline borates have been performed on boracites doped with paramagnetic elements [5–7]. In a recent study by Haddad *et al* the radiation-induced centres in the boron-oxygen framework of several boracite crystals were investigated [8]. It seemed interesting to investigate radiation-induced paramagnetic centres in a $Zn_4B_6O_{13}$ crystal. The crystal structure of this compound is relatively simple which reduces the number of possible radiation-induced centres. Upon UV irradiation anhydrous zinc metaborate shows a violet emission with a strong afterglow. The afterglow indicates the presence of thermally unstable, trapped charge carriers at room temperature after UV irradiation. In this study the UV-induced centres in $Zn_4B_6O_{13}$ are analysed by photoluminescence, thermoluminescence and temperature dependent EPR measurements on a single crystal. An earlier study on paramagnetic centres in UV-irradiated $Zn_4B_6O_{13}$ by Otero de la Gandara *et al* was performed on powdered material [9]. Especially at low temperatures, where

0953-8984/90/296303 + 11 $03.50

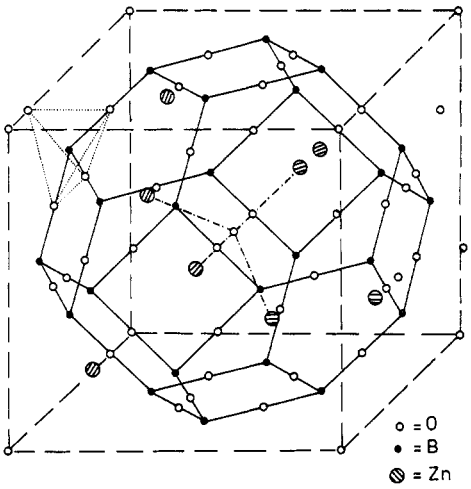

Figure 1. Schematic representation of the unit cell of $Zn_4B_6O_{13}$, after [13]. The O_{II} atoms of the BO_4 tetrahedra are depicted at the middlepoints of the edges, although they are not coplanar with the hexagonal faces. The 'free' O_I atoms are located in the centre and on the corners of the unit cell. The coordination of B by O_{II} and of O_I by Zn are indicated by · · · and – · –, respectively.

the EPR signals of several paramagnetic centres overlap, a reliable analysis of the EPR powder spectra is difficult. This is probably the main reason for the observed discrepancies between the present results and the results in [9]. Four types of paramagnetic centres were identified by us. Information on their thermal stability from the temperature dependent EPR measurements is correlated with the thermoluminescence properties.

The crystal structure of $Zn_4B_6O_{13}$, reported in [10, 11], is shown in figure 1. It is a sodalite-like structure in which the sodium atoms are replaced by zinc atoms, the silicon and aluminium by boron atoms and the chlorine atoms by oxygen. In this structure all boron atoms are four-coordinated by oxygen. The borate tetrahedra are linked to each other forming a three-dimensional framework. The zinc atoms are coordinated by three oxygen atoms of the borate framework and a free oxygen atom. The free oxygen atom O_I is coordinated by four zinc atoms. In this structure there are twelve times more oxygen atoms belonging to the borate framework, O_{II}, than free oxygen atoms, O_I.

2. Experimental details

The Czochralski grown single crystal of composition $Zn_4B_6O_{13}$ was kindly provided by Professor J Liebertz, University of Cologne. It was prepared according to the description given in [12]. The single crystal of $1 \times 2 \times 3$ mm^3 was oriented using a Polaroid XR-7 goniometer system. EPR spectra were recorded with a Varian E-6 spectrometer at 9.2 GHz (X-band) equipped with a liquid helium flow cryostat. The first derivative of the absorption spectrum was recorded with respect to the magnetic field. The microwave frequency was measured by a Hewlett-Packard frequency counter. A low microwave power (~2 mW) was used to avoid EPR line saturation. The sample was irradiated through quartz windows using a 450 W Xenon lamp.

Photoluminescence and thermoluminescence measurements were performed using a Perkin-Elmer MPF 44B spectrofluorometer, equipped with a liquid helium flow cryostat for measurements below room temperature (RT) and with a home-made high-temperature cell for measurements above RT. For linear heating in the thermoluminescence measurements a Newport Oxford sweep unit was used in the low-temperature regime (4–300 K) and a West 2050 temperature controller in the high temperature regime (300–600 K).

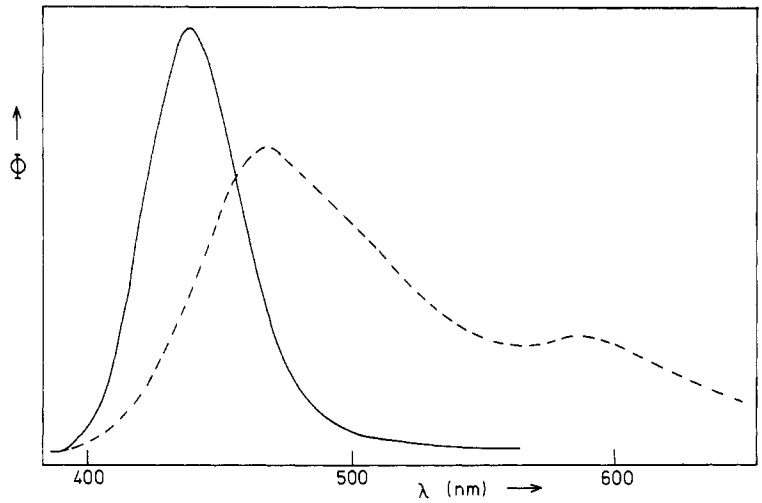

Figure 2. Emission spectrum of $Zn_4B_6O_{13}$ at 4.2 K for 250 nm excitation (——) and 290 nm excitation (– – –). Φ gives the spectral radiant power per constant wavelength interval.

3. Results

3.1. Photoluminescence and thermoluminescence

Upon UV irradiation the $Zn_4B_6O_{13}$ crystal shows a violet emission with a strong afterglow at RT. The emission spectrum, shown in figure 2, consists of a broad band with a maximum around 440 nm at 4.2 K which shifts to slightly shorter wavelength (435 nm) at 300 K. This spectrum is similar to the spectrum obtained by Terol and Otero for polycrystalline material [13]. The quenching temperature of the emission is high: no temperature quenching is observed until 400 K.

The excitation spectrum of the violet emission at 4 K and 300 K is shown in figure 3. The excitation spectrum at 4 K shows an asymmetrical band with a sharp edge on the longer wavelength side and a maximum at 250 nm. At RT the edge on the longer wavelength side is less sharp. Next to this dominant band in the excitation spectrum, there is a weak broad band around 290 nm. The relative intensity of this weak band is higher at lower temperatures. After extensive UV irradiation it tends to become stronger. Excitation in the 290 nm band gives a broad emission band with a maximum at 470 nm and a shoulder around 590 nm, shown in figure 2.

The emission spectrum of the afterglow is similar to the emission spectrum upon 250 nm excitation. The glow curve for the 440 nm emission between 4 and 300 K after UV irradiation (250 nm) at 4 K is shown in figure 4(*a*). Between 4 and 35 K a weak signal is observed, indicating the presence of some shallow traps. Around 80 K a small TL peak with a shoulder at 92 K is observed. In the temperature region 100 to 170 K no TL peaks are present. Between 170 and 300 K there are three about equally strong TL peaks with maxima at 215 K, 245 K and 270 K. The relative intensity of the three peaks depends on the irradiation time. The thermal trap depths for the 80 K and the 215 K bands have been determined, using the initial rise method [14], to be 0.14 eV and 0.49 eV, respectively. Attempts to characterise the traps with the transient thermoluminescence method [15] failed because the measurements of the decay of the luminescence intensity with time

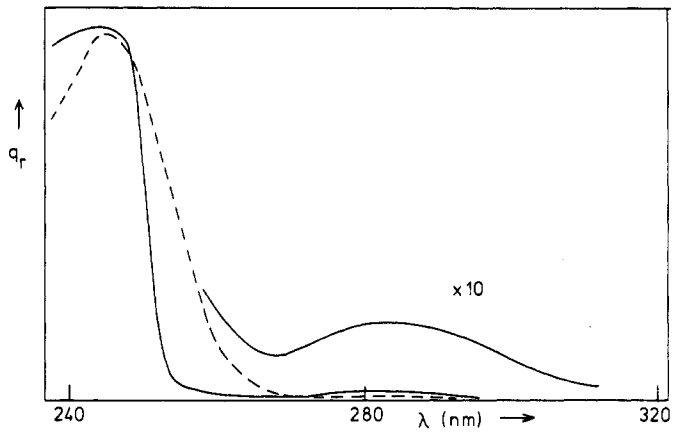

Figure 3. Excitation spectra of $Zn_4B_6O_{13}$ at 4.2 K (——) and 300 K (– – –) for 440 nm emission. q_r gives the relative quantum output.

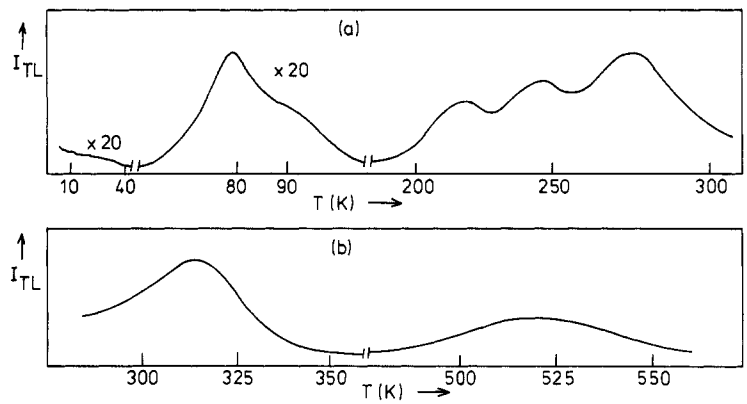

Figure 4. (*a*) Glow curve of the 440 nm emission of $Zn_4B_6O_{13}$ after 10 min UV irradiation (250 nm) at 4.2 K. The heating rate β is 0.1 K s^{-1}. (*b*) Glow curve of the 440 nm emission of $Zn_4B_6O_{13}$ after 10 min UV irradiation (250 nm) at 300 K. The heating rate β is 0.08 K s^{-1}.

after UV irradiation for different temperatures turned out to be non-reproducible. The reason for this observation is probably the dependence of the relative numbers of filled traps on previous UV irradiations.

In the glow curve above RT, figure 4(*b*), a TL peak around 320 K is observed next to some afterglow due to the 270 K peak. A weak TL peak is observed at 520 K.

3.2. EPR

Before irradiation no EPR signal could be detected. After UV irradiation at 15 K the EPR spectra show the presence of several types of radiation-induced paramagnetic centres. Four types of centres have been identified. The EPR lines corresponding to the different

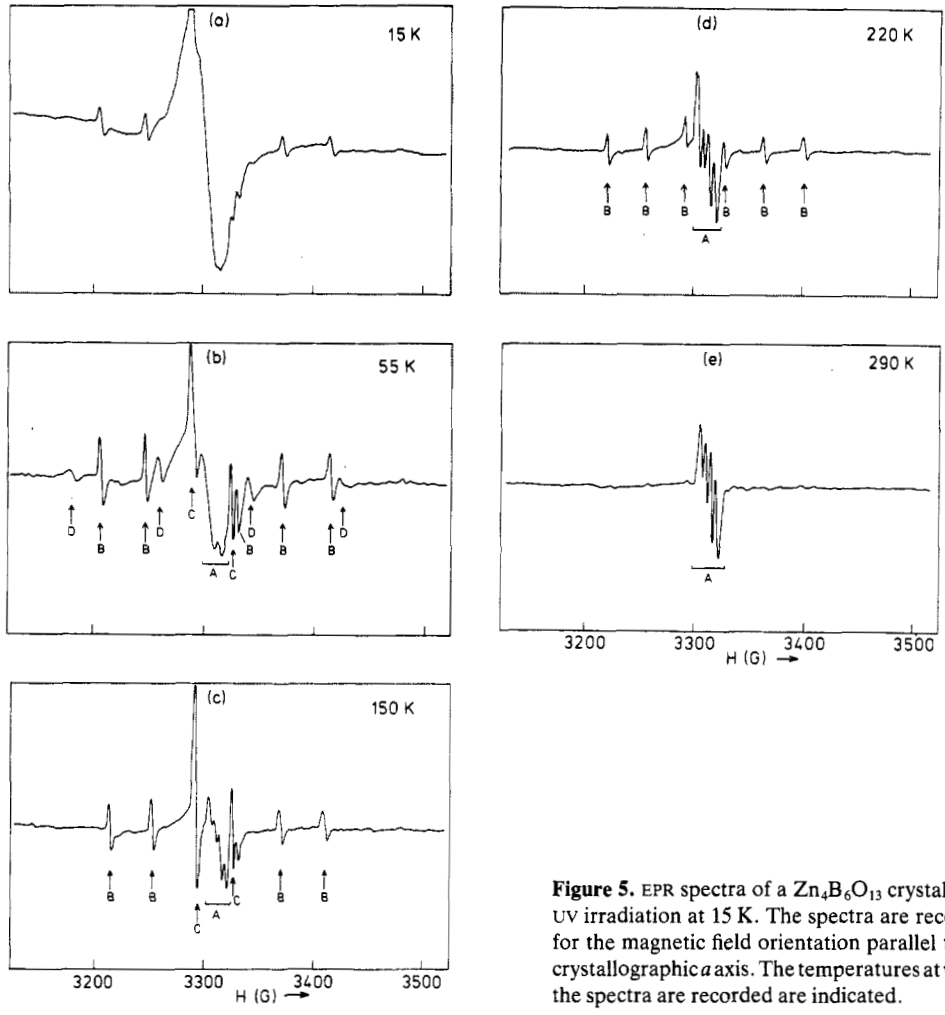

Figure 5. EPR spectra of a $Zn_4B_6O_{13}$ crystal after UV irradiation at 15 K. The spectra are recorded for the magnetic field orientation parallel to the crystallographic *a* axis. The temperatures at which the spectra are recorded are indicated.

centres have been marked by A, B, C and D in figure 5. In this figure the EPR spectra recorded for the static magnetic field parallel to the crystallographic *a* axis at several temperatures between 15 and 300 K are shown. Upon heating, after UV-irradiation at 15 K, the different EPR signals disappear, until only signal A is left at room temperature.

Signal A shows a four-line hyperfine structure. This is due to interaction of the electron spin with the ^{11}B nuclear spin ($I = 3/2$). Otero *et al* [9] have analysed signal A for a polycrystalline $Zn_4B_6O_{13}$ sample. The absence of overlapping EPR signals makes a reliable analysis of the EPR powder spectrum possible. The analysis by Otero resulted in a centre with axial symmetry with $g_\perp = 1.996$ and $g_\parallel = 2.002$. The hyperfine interaction parameters for interaction with the ^{11}B nuclear spin were found to be $A_\perp = 4$ G and $A_\parallel = 9$ G. The signal was assigned to an electron trapped in a O_{II} vacancy. This assignment is based on the *g*-value being smaller than g_e, which indicates the trapping of an electron, and the presence of the hyperfine interaction with the ^{11}B nuclear spin which indicates that the paramagnetic centre is located in a borate group.

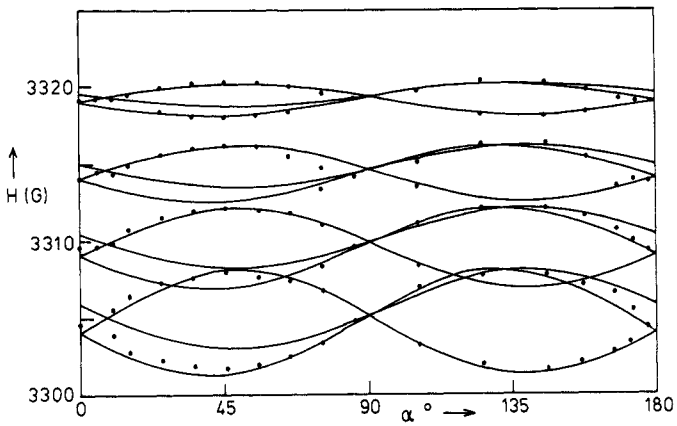

Figure 6. Angular variation of the EPR lines of signal A for the magnetic field perpendicular to the crystallographic *b* axis. α is the angle between the magnetic field and the *a* axis. The drawn lines are fits to (1).

In figure 6 the angular variation of the EPR lines of signal A is depicted for rotation along the *b* axis with the magnetic field perpendicular to the *b* axis. These data show the presence of at least two different orientations for the paramagnetic defect, resulting in two sets of four line spectra with a different angular dependence. For an electron trapped in an O_{II} vacancy four different orientations are possible when the principle axis for this centre is along the B–O bond. The angular variation for rotation along the *b* axis can be calculated for the centres of which the orientation is characterised by polar angles θ, the angle between the crystallographic *b* axis and the axis of the paramagnetic centre, and φ, the angle between the crystallographic *a* axis and the projection of the axis of the paramagnetic centre on the *ac* plane. From the crystallographic data the angles θ and φ have been calculated for the case of the magnetic field perpendicular to the *b* axis for the four B–O axes. In a first approximation the hyperfine lines are located at:

$$H = (h\nu/g_{\text{eff}}\mu_b) + A_{\text{eff}}m_I \tag{1}$$

where, for rotation along the *b*-axis (16):

$$g_{\text{eff}} = g_{\parallel}^2 \sin^2\theta\cos^2(\alpha-\varphi) + g_{\perp}^2[1-\sin^2\theta\cos^2(\alpha-\varphi)]$$

$$A_{\text{eff}} = A_{\parallel}^2(g_{\parallel}^2/g_{\text{eff}}^2)\sin^2\theta\cos^2(\alpha-\varphi) + A_{\perp}^2(g_{\parallel}^2/g_{\text{eff}}^2)[1-\sin^2\theta\cos^2(\alpha-\varphi)]$$

where α is the angle between the magnetic field and the *a* axis.

For two of the four B–O orientations the calculated angular dependence is identical, resulting in one set of four lines. The other two orientations have related angular dependences, resulting in two sets of four lines situated closely together. Due to the width of the hyperfine lines the latter two sets of four lines are observed experimentally as one set of four lines at values in between the calculated lines. In figure 6 the three calculated sets of four lines for the best fit are shown together with the experimental data. The best fit between the observed and the calculated angular dependence, as determined by eye, is obtained for $g_{\perp} = 1.996$, $g_{\parallel} = 2.000$, $A_{\perp} = 4$ G and $A_{\parallel} = 6$ G. The values are in fairly good agreement with the values of Otero *et al* [9]. Thus signal A can be assigned to a paramagnetic centre due to an electron trapped in an O_{II} vacancy of which the principle axes are located along the B–O axes.

The A-signal is the only signal stable at RT. To test the thermal stability of the

paramagnetic centre the sample was heated outside the cryostat to some 100 °C. After the heating, signal A has disappeared completely.

Up to 250 K signal B can be observed next to signal A. Signal B consists of six hyperfine lines due to interaction with a nuclear spin of 5/2. The absence of atoms with $I = 5/2$ in $Zn_4B_6O_{13}$ implies that this signal is due to a paramagnetic centre connected with an impurity. The most probable candidate is Mn^{2+} on a Zn^{2+} site. Mn^{2+} has a nuclear spin of 5/2 and can be expected to be present as an impurity in the Zn starting material. Otero found a similar six-line structure around $g = 2.002$ with a hyperfine splitting of 40 G.

Rotation along the *b* axis reveals the presence of at least two magnetically non-equivalent sites. For the magnetic field parallel to the *a* axis the different sets of six hyperfine lines coincide. The lines are located around $g = 1.998$ for this orientation. The spacings between the six hyperfine lines are not identical: at 15 K the spacings range from 40.8 to 44.5 G and at 225 K from 34.5 to 36.7 G, the smaller spacings being observed on the stronger field side. The departure from even spacings between the hyperfine lines is due to a contribution of second order terms in the hyperfine coupling constant [17].

The average hyperfine coupling constant shows a marked decrease with increasing temperature from 42 G at 15 K to 35 G at 255 K. This effect is clearly observed in figure 5. A decrease of the hyperfine coupling constant with increasing temperature is a known effect. It has been observed for Mn^{2+} [18] and F-centre electrons [19]. Calculations by Simanek and Orbach [20] showed that this decrease is due to lattice vibrations. Coupling with phonons can reduce the isotropic contact interaction as well as the anisotropic dipole–dipole interaction [20, 21]. The small shift in Δg with temperature, expected on the basis of the same effect, has not been observed. The experimental inaccuracy is too large to observe this effect.

The *g* value being smaller than g_e suggests that signal B is due to a trapped electron. A possibility for the centre is Mn^+. Mn^{2+} can trap an electron and become Mn^+. EPR measurements on irradiated CaF_2–Mn^{2+} revealed the presence of Mn^+ centres with a similar thermal stability (200 K) and hyperfine splitting (30 G) as observed for the B signal [22].

Signal C is a strong signal without hyperfine structure. Up to about 170 K the signal is stable. In figure 7 the angular dependence of signal C for rotation along the *b* axis is shown. This picture shows that the centre is located in three magnetically non-equivalent sites. The sites are characterised by symmetry along the [100] axis. The values for $g_\parallel$ and $g_\perp$ determined from figure 7 are $g_\parallel = 1.9900$ and $g_\perp = 2.0105$. The solid line in figure 7 is a fit of the observed angular dependence to the theoretical angular dependence of *g*:

$$g^2 = g_\parallel^2 \cos^2 \alpha + g_\perp^2 \sin^2 \alpha. \tag{2}$$

The absence of hyperfine structure shows that the paramagnetic centre corresponding to signal C is not located in a borate group. Two possible candidates for this centre are an electron trapped in an O_I vacancy or a hole trapped on O_I, giving O_I^-. There are two arguments that support the former possibility.

(i) The *g* values for an O^- centre are characterised by $g_\parallel \simeq g_e$ and $g_\perp > g_e$ [8, 23, 24]. The present results show a $g_\parallel$ significantly smaller than g_e. This suggests that signal C is not due to a trapped hole on O_I.

(ii) The A signal shows a small increase when signal C disappears around 170 K. This increase can be understood if signals A and C correspond to the same type of trap. Then a part of the thermally released charge carriers from signal C can be retrapped by the

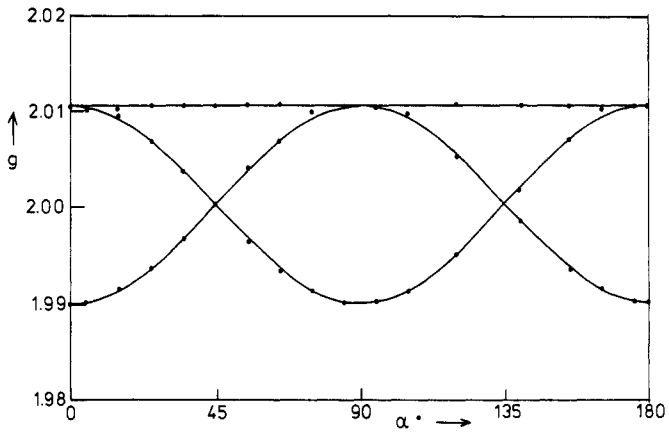

Figure 7. Angular variation of the EPR lines corresponding to signal C. The magnetic field is perpendicular to the *b* axis and α is the angle between the magnetic field and the crystallographic *a* axis. The drawn lines are fits to (2).

centre corresponding to signal A. This observation supports the assignment of signal C to a trapped electron, just as with signal A.

In view of these arguments signal C is assigned to an electron trapped in an O_I vacancy. The results obtained by Otero *et al* are different from our observations: they observed two axial signals without HFS. A signal with $g_\parallel = 1.993$ and $g_\perp = 1.997$ was assigned to an electron trapped in an O_I vacancy and a signal with $g_\parallel = 2.003$ and $g_\perp = 2.017$ was assigned to a hole trapped on O_I [9]. Since the EPR spectra corresponding to the two signals without HFS are not shown in [9], it is difficult to find the origin of the discrepancy. The reason may be that the presence of several overlapping signals inhibits a reliable analysis of the EPR powder spectra.

Signal D is not very stable. It disappears at about 130 K. The signal shows a four-line hyperfine structure due to interaction with a ^{11}B nuclear spin. The four lines are located around $g = 2.0030$ for the magnetic field parallel to the *a* axis. The hyperfine splitting parameter is large, 80 G. Similar large hyperfine splittings for interaction with a ^{11}B nuclear spin have been reported for an electron trapped by B^{3+} of a borate group in alkali borate glasses [2] and in boracites [8]. The trapping of the electron is assumed to take place in a dangling bond of three-coordinated boron. In the case of four-coordinated boron the trapping of an electron by boron is unlikely [2]. Since all boron atoms are four-coordinated by oxygen in $Zn_4B_6O_{13}$, signal D cannot be assigned to an electron trapped by a borate group. It seems more probable that the EPR signal is due to a hole trapped by a borate group. Also the *g*-value, which is larger than g_e, suggests that signal D corresponds to a trapped hole.

At low temperatures (15 K) the different signals around g_e are obscured by a broad band ($\approx$ 28 G). This broad signal is probably due to paramagnetic centres with $g \simeq g_e$ corresponding to different shallow traps which are stable only at cryogenic temperatures. After heating the sample to 50 K the broad band around g_e has completely disappeared and the EPR spectrum showing signals A, B, C and D is observed.

4. Discussion

The violet emission band, observed in photoluminescence and thermoluminescence, is

an intrinsic property of undoped $Zn_4B_6O_{13}$. The exact nature of this emission band is unknown. The results show that the emission may result from a strongly localised self trapped exciton (STE) state. The asymmetrical excitation band with a sharp edge on the longer-wavelength side suggests bandgap excitation, which can be expected for STE emission. The large Stokes shift (2 eV) indicates that the STE is strongly localised due to large lattice relaxation. The large lattice relaxation is consistent with the high quenching temperature for the luminescence. In the case of weak lattice relaxation the STE will become mobile at a relatively low temperature, resulting in the quenching of the STE emission [25]. The results on the luminescence of $Zn_4B_6O_{13}$ are comparable with, for example, the STE luminescence reported for β-Ga_2O_3 [25]. Many Ga^{3+}-borates show a similar luminescence [26]. They are more or less isoelectronic with $Zn_4B_6O_{13}$.

The weak band in the excitation spectrum at 290 nm can be ascribed to defects. The influence of UV irradiation on the relative intensity of this excitation band suggests that it is related to UV-induced centres. This is in line with the observed increase of the relative intensity of this band at low temperatures, where the UV-induced centres are thermally stable. The emission bands associated with the defects are shifted to longer wavelengths, 470 nm and 590 nm, with respect to the intrinsic emission band. No attempts have been made to correlate the defect excitation and emission bands with the paramagnetic centres observed in EPR.

Very little research has been performed on the luminescence of undoped borates. Recently Valbis *et al* reported on the luminescence of undoped BaB_2O_4 [27]. Their results are in line with our results: upon bandgap excitation (160 nm) they observed a strongly Stokes shifted emission band (295 nm), which was tentatively ascribed to STE emission. Next to this band other emission bands with complicated excitation spectra were observed and ascribed to defects or impurities.

The glow curve is clearly related to the thermal stability of the paramagnetic centres: TL peaks start at temperatures at which the EPR signals of paramagnetic centres disappear. During the temperature dependent EPR measurements the sample was kept for a rather long time (30–60 min) at constant temperature to perform angular dependent measurements. Due to this the disappearance of EPR signals is observed at temperatures which correspond to the onset of the TL peaks, where a slow depletion of the traps starts. These temperatures are considerably lower than the temperatures corresponding to the maxima of the TL peaks in the glow curves, recorded with a heating rate of 0.1 K s^{-1}.

Three of the four EPR signals analysed are related to peaks in the TL spectrum. The vanishing of signal C, ascribed to an electron trapped in an O_I vacancy, at 170 K corresponds to the TL peak starting at 170 K with a maximum at 215 K. Signal B, due to an electron trapped on or near Mn^{2+} impurities, disappears at 250 K, suggesting a relation with the TL peak around 270 K. Finally signal A disappears in the temperature regime where the TL peak at 320 K is observed. All these three EPR signals are ascribed to trapped electrons. The thermally released electrons recombine with trapped holes to give the intrinsic violet emission. The nature of the hole trap is not clear. The absence of an EPR signal due to the trapped hole shows that the trapped hole centres are either diamagnetic or have g-values below 1.97 or above 2.03.

The two signals ascribed to an electron trapped in an oxygen vacancy have a different thermal stability. The electron trapped in an O_{II} vacancy in the borate framework is thermally more stable than the electron trapped in the O_I vacancy. This is to be expected: the electron will be more tightly bound in the borate group by trivalent boron than in the O_I vacancy by divalent zinc. Also, the shorter Zn–O_{II} distance (1.957 Å) compared

to the Zn–O_I distance (1.982 Å) indicates that an electron trapped in the O_I vacancy will be bound less strongly than an electron trapped in an O_{II} vacancy. The same holds for the oxygen atoms: it will be energetically less favourable to create an O_{II} vacancy in the borate framework than to create an O_I vacancy. This explains why the EPR signals due to electrons trapped in O_I and O_{II} vacancies are about equally strong, although there are twelve times more O_{II} sites than O_I sites in the unit cell.

No TL peak is observed around 130 K where signal D disappears. Although signal D is weak, a peak in the TL spectrum can be expected, unless the larger part of the thermally released charge carriers is retrapped or recombines non-radiatively. The reason for the absence of a TL peak may be connected to signal D being due to a trapped hole, unlike the other EPR signals which do correspond to a peak in the TL spectrum. In the case of efficient retrapping of the thermally released holes by the unknown deep hole traps no TL peak is expected. Another possibility is that recombination of the thermally released holes and trapped electrons gives emission at a wavelength different from the 440 nm for which the TL spectrum has been recorded. The disappearance of the broad EPR signal around g_e at low temperatures is accompanied by a very small peak between 4 and 35 K in the TL curve. This TL peak is too small to explain the rather strong EPR signal around g_e. The explanation for the absence of a strong TL peak is probably similar to the explanation for the absence of a TL peak corresponding to signal D.

Three peaks in the TL spectrum, around 80 K, 245 K and 520 K, seem not to be related to a signal in the EPR spectrum. The 80 K TL peak is very weak and a weak EPR signal may be hidden under the different strong EPR signals. EPR signals corresponding to the 245 K and 520 K TL peaks would be strong enough to be observable if these peaks were due to a paramagnetic centre with a g-value in the range 1.97 to 2.03. Apparently this is not the case.

5. Conclusions

The photoluminescence properties of $Zn_4B_6O_{13}$ show that the intrinsic violet emission of this material may originate from a strongly localised self-trapped exciton state. Upon UV irradiation at low temperatures only a part of the created free charge carriers recombine directly to give the intrinsic violet emission. The other part is trapped in electron traps and hole traps. Four types of UV-induced paramagnetic centres could be identified. The three strongest signals are assigned to electrons trapped in 'free' O_I vacancies, in 'borate' O_{II} vacancies and on or near Mn^{2+} impurities. At temperatures at which these paramagnetic centres become thermally unstable and disappear, the onset of peaks in the glow curve is observed. The electrons trapped by $V_{O_I}^{\cdot\cdot}$, Mn^{2+} and $V_{O_{II}}^{\cdot\cdot}$ give TL peaks at 215 K, 270 K and 320 K, respectively. The fourth EPR signal, which disappears around 130 K, is assigned to a hole trapped by a borate group. The major part of the trapped holes is not observed in EPR, suggesting that these centres are either diamagnetic or have g-values outside the range studied.

Acknowledgments

The authors are indebted to Professor J Liebertz for providing the single crystal and to Mr R Sitters for the assistance during the EPR measurements.

References

[1] Stoneham A M 1975 *Theory of Defects in Solids* (Oxford: Oxford University Press) ch 13
[2] Griscom D L 1971 *J. Chem. Phys.* **55** 1113
[3] Taylor P C, Griscom D L and Bray P J 1971 *J. Chem. Phys.* **54** 748
[4] Kishii T and Ooka K 1967 *J. Phys. Soc. Japan* **23** 659
[5] Petrov M P, Kizhaev S A, Andreeva G T and Smolensky G A 1970 *J. Phys. Soc. Japan* **28** suppl 128
[6] Rivera J P, Bill H and Lacroix R 1976 *Phys. Status Solidi* a **35** K105
[7] Rivera J P, Bill H and Lacroix R 1988 *Ferroelectrics* **80** 31
[8] Haddad M, Vignaud G, Berger R and Levasseur A 1985 *J. Phys. Chem. Solids* **46** 997
[9] Otero de la Gandara M J, Conesa J C and Soria J 1985 *Phys. Status Solidi* a **87** K81
[10] Smith P, Garcia-Blanco S and Rivoir L 1964 *Z. Kristallogr.* **119** 375
[11] Smith-Verdier P and Garcia-Blanco S 1980 *Z. Kristallogr.* **151** 175
[12] Bohaty L, Haussühl S, Liebertz J and Stahr S 1982 *Z. Kristallogr.* **161** 157
[13] Terol S and Otero M J 1961 *Z. Naturf.* **169** 920
[14] McKeever S W S 1985 *Thermoluminescence in Solids* (Cambridge: Cambridge University Press)
[15] Nakazawe E 1984 *Japan. J. Appl. Phys.* **23** L755
[16] McGarvey B R 1966 *Transition Metal Chemistry* vol 3 ed R L Carlin (New York: Marcel Dekker) p 122
[17] Pake G E 1962 *Paramagnetic Resonance* (New York: Benjamin) p 78
[18] Walsh W M Jr, Jeener J and Bloembergen N 1965 *Phys. Rev.* **139** A1338
[19] Seidel H 1961 *Z. Phys.* **165** 218
[20] Simanek E and Orbach R 1966 *Phys. Rev.* **145** 191
[21] Dreybrodt W 1967 *Phys. Status Solidi* **21** 99
[22] Jahan M S and Cooke D W 1984 *Phys. Status Solidi* b **126** 687
[23] Wong N and Lunsford J 1971 *J. Chem. Phys.* **55** 3007
[24] Schirmer O F 1971 *J. Phys. Chem. Solids* **32** 499
[25] Harwig T, Kellendonk F and Slappendel S 1978 *J. Phys. Chem. Solids* **39** 675
[26] Blasse G and Bril A 1970 *Mater. Res. Bull.* **5** 231 and references therein
[27] Valbis Y A, Ivleva L J, Kuzminov Y S, Payats V A and Springis M E 1989 *Opt. Spectrosc. (USSR)* **66** 177